

# $R^2$ -Mesh: Reinforcement Learning Powered Mesh Reconstruction via Geometry and Appearance Refinement

Haoyang Wang, Liming Liu, Quanlu Jia, Jiangkai Wu, Haodan Zhang, Peiheng Wang, Xinggong Zhang\*

Peking University

## Abstract

Mesh reconstruction based on Neural Radiance Fields (NeRF) is popular in a variety of applications such as computer graphics, virtual reality, and medical imaging due to its efficiency in handling complex geometric structures and facilitating real-time rendering. However, existing works often fail to capture fine geometric details accurately and struggle with optimizing rendering quality. To address these challenges, we propose a novel algorithm that progressively generates and optimizes meshes from multi-view images. Our approach initiates with the training of a NeRF model to establish an initial Signed Distance Field (SDF) and a view-dependent appearance field. Subsequently, we iteratively refine the SDF through a differentiable mesh extraction method, continuously updating both the vertex positions and their connectivity based on the loss from mesh differentiable rasterization, while also optimizing the appearance representation. To further leverage high-fidelity and detail-rich representations from NeRF, we propose an online-learning strategy based on Upper Confidence Bound (UCB) to enhance viewpoints by adaptively incorporating images rendered by the initial NeRF model into the training dataset. Through extensive experiments, we demonstrate that our method delivers highly competitive and robust performance in both mesh rendering quality and geometric quality.

## 1 Introduction

Mesh reconstruction of 3D scenes is profoundly essential in domains such as virtual reality (Navarro et al. 2018), medical imaging (Kong, Wilson, and Shadden 2021) and robotics (Lu et al. 2023). However, reconstructing meshes from RGB images poses significant challenges due to issues including occlusions, varying lighting conditions and texture details necessary for high-quality 3D models.

In recent years, the emergence of Neural Radiance Fields (NeRF) (Mildenhall et al. 2020; Müller et al. 2022; Fridovich-Keil et al. 2023) has marked a breakthrough in the field of 3D reconstruction. NeRF’s exceptional ability to model the volumetric density and appearance of scenes from sparse sets of images has opened up new avenues for enhancing mesh reconstruction. Building on this foundational work, numerous researchers integrate NeRF’s capabilities to advance the reconstruction of meshes.

MobileNeRF (Chen et al. 2023) explicitly initializes a polygonal mesh as a regular grid. The mesh is then pro-

gressively optimized through the NeRF model, which efficiently predicts volumetric densities and color properties at ray-mesh intersection points within the scene. However, the connectivity between vertices is fixed, and only the positions of the vertices can be updated during training. This limits the adaptability of the mesh structure to complex geometries, resulting in suboptimal geometric outcomes in the final mesh. Alternatively, some recent works (Wang et al. 2021, 2023; Rakotosaona et al. 2024) transform radiance fields into Signed Distance Fields (SDF) to represent more accurate surface positions. These methods extract the final polygonal meshes by Marching Cubes (Lorensen and Cline 1998) which may lead to poor geometric quality and rendering quality. NeRF2Mesh (Tang et al. 2023) employs a differentiable rasterizer to optimize mesh vertex positions and face density based on rendering loss. However, the connectivity between vertices cannot be freely updated, limiting the mesh geometric performance.

To address these challenges, we propose a novel algorithm that progressively generates and optimizes meshes from multi-view images. Specifically, our approach initiates with the efficient training of a NeRF model to establish an initial Signed Distance Field (SDF) and a view-dependent appearance field. To enable flexible updates of mesh vertices and edges, we employ FlexiCubes (Shen et al. 2023) to extract a mesh from the learned SDF. Subsequently, we use a differentiable rasterization technique (Munkberg et al. 2022) to continuously optimize the SDF and the appearance field based on rendering losses, enabling the iterative updating of the extracted mesh.

Due to the superior rendering capabilities of NeRF, which can capture complex lighting and detailed textures, we further incorporate images rendered by the initial NeRF model into the training dataset for mesh training. We propose an online reinforcement learning strategy based on the Upper Confidence Bound (UCB) algorithm (Auer, Cesa-Bianchi, and Fischer 2002) to adaptively enhance viewpoints. This strategy explores and selects the optimal combination of viewpoints online, based on the rendering performance in the validation set during mesh training, ultimately leading to more accurate and realistic mesh geometric reconstruction. Additionally, our adaptive viewpoint enhancement strategy is general and can be applied to any mesh generation framework that includes an initial trained NeRF model. The over-

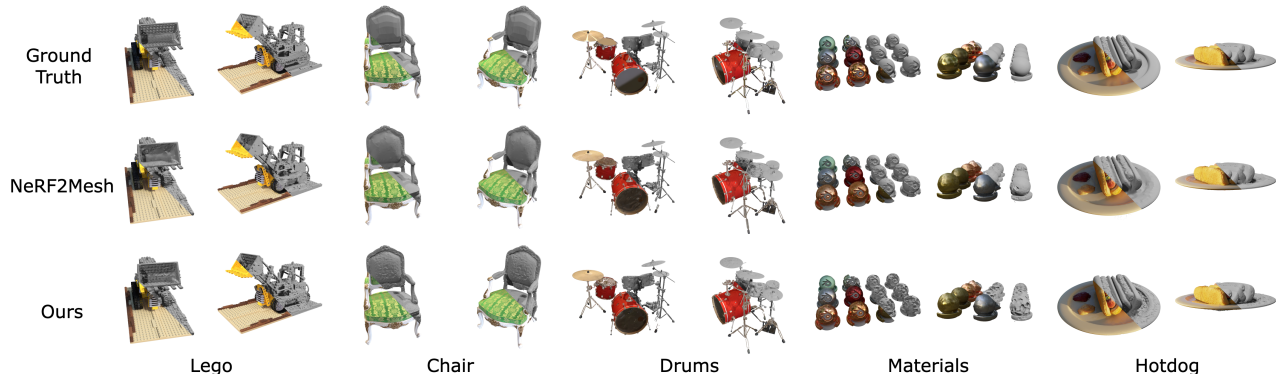


Figure 1: Visualization of our overall performance. Our method achieves highly competitive and robust performance in both mesh rendering quality and geometric quality.

all performance of our method is depicted in Figure 1.

In summary, the key contributions of our work are as follows:

- We present a novel algorithm for mesh reconstruction from multi-view images that iteratively refines both geometry and appearance while allowing for the flexible adjustment of mesh vertices and edges, achieving excellent geometric outcomes.
- We propose an online reinforcement learning strategy based on the Upper Confidence Bound (UCB) algorithm to enhance viewpoints by adaptively selecting the optimal combination of viewpoints from images rendered by the initial NeRF model to enhance the dataset, thereby improving the quality of mesh rendering.
- Our adaptive viewpoint enhancement strategy is general and can be applied to any mesh reconstruction framework that includes an initial trained NeRF model.
- Our mesh refinement algorithm, combined with the online UCB strategy, demonstrates competitive performance in both rendering quality and mesh reconstruction, showcasing the effectiveness of our approach in producing high-fidelity visual and geometric results.

## 2 Related Work

### 2.1 Mesh Reconstruction from NeRF

NeRF (Mildenhall et al. 2020) and its variants (Müller et al. 2022; Chen et al. 2022; Fridovich-Keil et al. 2022; Sun, Sun, and Chen 2022) significantly advance 3D scene reconstruction through a volumetric scene function learned from multi-view images. Some works explore the possibility of generating meshes simultaneously during the training of NeRF models. A notable example is MobileNeRF (Chen et al. 2023). However, the generated polygonal mesh lacks surface smoothness since the mesh topology is fixed at the initial stage. Most recent studies (Wang et al. 2021, 2023; Long et al. 2022; Yariv et al. 2021; Oechsle, Peng, and Geiger 2021; Munkberg et al. 2022; Hasselgren, Hofmann, and Munkberg 2022) adopt SDF to represent geometric surfaces. Some of these works (Wang et al. 2021, 2023; Long et al. 2022; Yariv et al. 2021; Oechsle, Peng,

and Geiger 2021) leverage the ray-marching volumetric rendering formula of NeRF, optimize the SDF to achieve accurate scene representations. They then apply classical iso-surfacing algorithms, such as Marching Cubes (Lorenson and Cline 1998) and Dual Contouring (Ju et al. 2002), to extract the mesh. However, this post-extraction leads to loss of detail and surface artifacts that degrade the quality of the extracted mesh. Some studies conduct mesh refinement processes to further enhance the geometric quality. NVdiffrec (Munkberg et al. 2022) utilizes mesh differentiable surface rendering to optimize the SDF, but due to the random initialization of the SDF, it can lead to training instabilities and the presence of floating artifacts. NeRF2Mesh (Tang et al. 2023) performs mesh refinement by optimizing the vertices' positions and face density based on rendering errors, but the connectivity between vertices cannot be fully adjusted. Our approach ensures a well-initialized representation of the scene and maintains flexible adjustments of vertices and their connectivity during the mesh refinement process.

### 2.2 Best Views Selection in 3d Scenes

Selecting best views in 3d scenes is a critical issue in computer vision and 3D reconstruction, directly impacting the quality of final rendering and model reconstructions. Traditional approaches often rely on heuristic or predetermined viewpoint strategies, which may not adapt well to dynamically changing environments or complex scene structures. Some recent works (Pan et al. 2022; Kim et al. 2024; Jin et al. 2023) in radiance fields incorporate uncertainty estimation to guide the selection process. However, these approaches are based on ray sampling in radiance fields training, which are less applicable to our focus on surface mesh reconstruction. Additionally, several studies concentrate on the field of next best view (NBV) planning (McGreavy, Kunze, and Hawes 2017; Naazare, Rosas, and Schulz 2022; Krainin, Curless, and Fox 2011), which is primarily applied in the robotic exploration of unknown environments. These works aim to optimize the reconstruction of the new scene by selecting the minimal number of viewpoints necessary for comprehensive coverage. However, our objective is to enhance the observational perspective by online selecting the

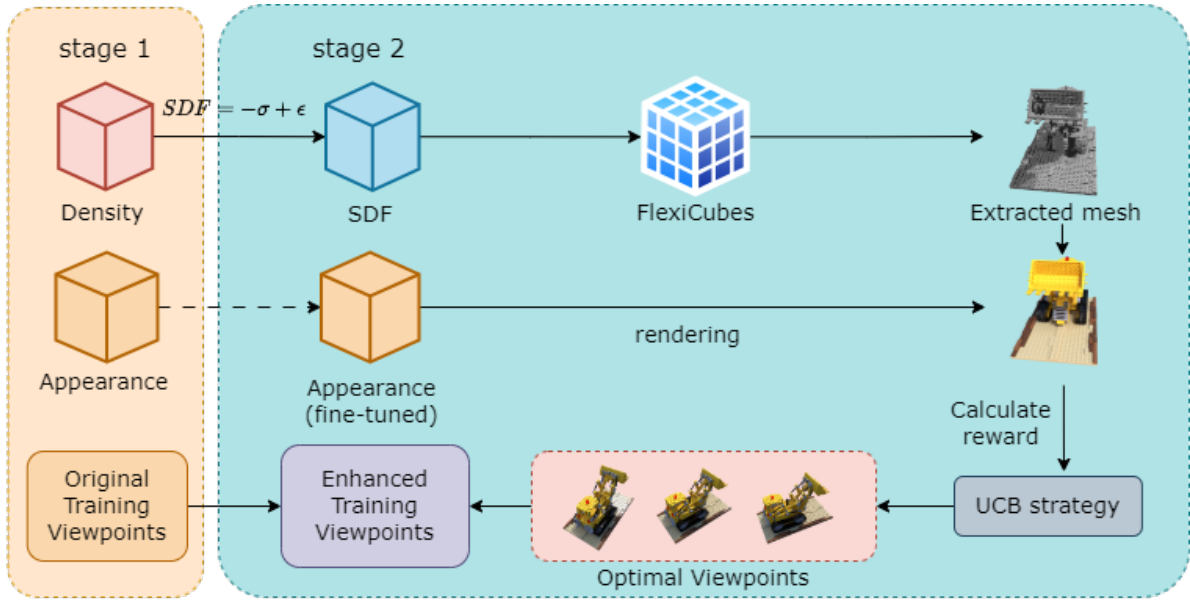


Figure 2: Our Framework. In stage 1, we initialize the geometry and view-dependent appearance representation based on NeRF. This initial phase results in a coarse SDF grid and a set of candidate viewpoints rendered by NeRF model for enhancement in the subsequent stage. Then in stage 2, for each training iteration, we take two steps. We first select the optimal combination of viewpoints based on UCB strategy to incorporate into the training dataset. We then simultaneously refine both the geometry and the appearance representation. After training is complete, we obtain the final mesh.

optimal combination of candidate viewpoints based on existing training viewpoints and their performance gains.

### 3 Method

#### 3.1 Framework

In this section, we introduce our framework,  $R^2$ -mesh, as illustrated in Figure 2. We adopt a two-stage training process for mesh reconstruction. In stage 1, following the approach of NeRF2Mesh, we utilize Instant-NGP (Müller et al. 2022) as the primary architecture to initialize the geometry and view-dependent appearance of the mesh (Section 3.2). This initial phase results in a coarse SDF grid and a set of candidate viewpoints rendered by NeRF model for enhancement in the subsequent stage. Then in stage 2, for each training iteration, we take two steps. We first select the optimal combination of viewpoints based on UCB values to incorporate into the training dataset (Section 3.3). We then simultaneously refine both the geometry and the appearance representation (Section 3.4). Upon completion of the training, we employ the NeRF2Mesh methodology to export a textured surface mesh.

#### 3.2 Efficient 3d Scene Initialization (Stage 1)

In the first stage, we utilize the NeRF2Mesh approach which is based on the Instant-NGP architecture to efficiently train a NeRF model for initializing 3D scene information. The geometry is learned through a multi-resolutional density grid combined with a shallow Multilayer Perceptron (MLP). The

appearance representation is decomposed into diffuse colors and view-dependent specular features. For each ray, at every sampling point, the specular feature is transformed into specular color using a shallow MLP that takes into account the direction of the ray. The resulting diffuse and specular color are then combined to create the final color of a sampling point. After the specular and diffuse colors are computed at each sampling point along a ray, the rendering process uses volumetric rendering techniques to integrate these colors along the ray’s path to produce the final pixel color by using the following equation:

$$C(r) = \sum_{i=1}^N T_i (1 - \exp(-\sigma_i \Delta t_i)) \mathbf{c}_i \quad (1)$$

where  $C(r)$  is the accumulated color along ray  $r$ ,  $T_i$  is the transmittance from the camera to the  $i$ -th point, calculated as  $T_i = \exp\left(-\sum_{j=1}^{i-1} \sigma_j \Delta t_j\right)$ .  $\sigma_i$  represents the density at the  $i$ -th point,  $\Delta t_i$  is the distance between the  $i$ -th and  $(i+1)$ -th sampled points, and  $\mathbf{c}_i$  is the combined diffuse and specular color at the  $i$ -th point.

To optimize the NeRF model, an MSE loss is used to calculate the squared differences between the predicted and ground truth colors of the pixels:

$$L_{\text{MSE}} = \frac{1}{N} \sum_{i=1}^N (\hat{C}_i - C_i)^2 \quad (2)$$

	Lego	Hotdog	Chair	Drums	Ficus	Mic	Ship	Materials	Mean
NVdiffrec	1.9	3.1	9.4	3.4	0.6	1.0	38.4	1.2	7.38
Neus2	2.0	3.4	4.1	1.8	0.6	0.9	19.6	1.3	4.22
NeRF2Mesh	2.1	3.7	<b>1.0</b>	2.5	0.4	1.2	35.9	1.2	6.00
Ours	<b>1.6</b>	<b>3.1</b>	3.3	<b>1.6</b>	<b>0.4</b>	<b>0.8</b>	<b>10.4</b>	<b>0.5</b>	<b>2.71</b>

Table 1: Chamfer Distance ( $\downarrow$ ) in units of  $10^{-3}$  on the NeRF-synthetic dataset compared to the ground truth meshes. Our method achieves competitive results compared to other methods.

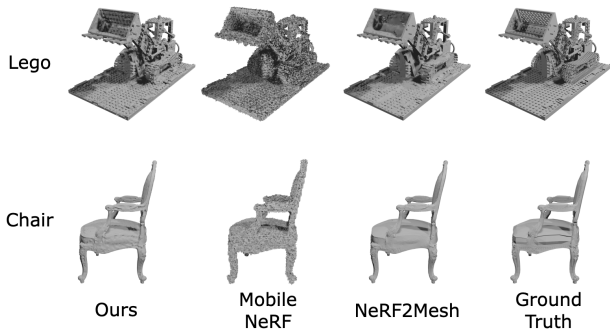


Figure 3: Mesh reconstruction quality on NeRF-synthetic dataset. Our results significantly outperform the previous works.

where  $\hat{C}_i$  is the predicted color and  $C_i$  is the ground truth color of the  $i$ -th pixel, with  $N$  representing the total number of pixels.

Following NeRF2Mesh, we apply L2 regularization on the specular color term to promote the separation of diffuse and specular color:

$$L_{\text{spec}} = \sum \|\mathbf{c}_{\text{spec}}\|^2 \quad (3)$$

where  $\mathbf{c}_{\text{spec}}$  represents the specular color of a sampling point.

After training is complete, we extract a density grid at the specified resolution and convert it into an SDF grid. Density represents the amount of material at a point and is inherently positive, while SDF values indicate the shortest distance to the nearest surface, allowing them to be both positive and negative to distinguish between exterior and interior regions. Therefore, we convert density values into a coarse SDF grid using the following simple formula:

$$\text{SDF} = -\sigma + \epsilon. \quad (4)$$

where  $\sigma$  represents the density value at a point, and  $\epsilon$  is a small positive number.

This transformation establishes our initial SDF grid, which we then further refine in stage 2.

### 3.3 UCB-based Adaptive Viewpoint Enhancement (Stage 2)

After stage 1 converges, we set up hundreds of rendered images as candidate viewpoints for stage 2 mesh refinement by rendering the entire scene from various angles. Our goal is to

select the optimal combination of viewpoints in each training iteration based on the performance gains from previous viewpoint selections.

Given a set of viewpoints  $V_{\text{nerf}} = \{v_1, v_2, \dots, v_n\}$  rendered by the initial NeRF, we aim to select the optimal combination of viewpoints  $V$ , which is an NP-hard problem. Therefore, to simplify the computational complexity, we group the nearest viewpoints together to reduce the search space.

During the training process, the model parameters and the rendering losses of each training viewpoint are continuously varying, it is not optimal to select a fixed set of viewpoints to enhance the dataset throughout the training process. To address this issue, we propose an online reinforcement learning (RL) strategy to adaptively select the optimal combination of viewpoints in each training iteration considering the current state of the model and the performance gains from previously selected viewpoint combinations.

Many state-of-the-art reinforcement RL methods, such as DQN (?) and PPO (Schulman et al. 2017), introduce additional networks for inference, which results in significant time overhead. In contrast, our strategy using UCB does not require neural networks for inference, thereby reducing computational complexity and speeding up the decision-making process.

In our strategy, we set all viewpoints from the training set  $V_{\text{train}}$  as the action space  $\mathcal{A}$ . The closest  $m$  viewpoints from the candidate set  $V_{\text{nerf}}$  to a training set viewpoint  $v_{\text{train},i} \in V_{\text{train}}$  are combined together as a single action in our RL strategy. The UCB value for each action is calculated as follows:

$$\text{UCB}_a(t) = \hat{r}_a(t) + c \sqrt{\frac{2 \ln t}{N_a(t)}} \quad (5)$$

where  $\hat{r}_a(t)$  represents the empirical mean reward for action  $a$  up to time  $t$ ,  $c$  is a constant controlling the degree of exploration,  $\ln t$  is the natural logarithm of the total number of steps  $t$ , and  $N_a(t)$  denotes the number of times action  $a$  has been selected. Here, time  $t$  specifically refers to the  $t$ -th iteration in the stage 2 training process. At initialization, the UCB value for each action is set to a large value, ensuring that every action is explored at least once.

For each training iteration, we select the optimal action that maximizes the UCB value:

$$a_t = \arg \max_a \text{UCB}_a(t) \quad (6)$$



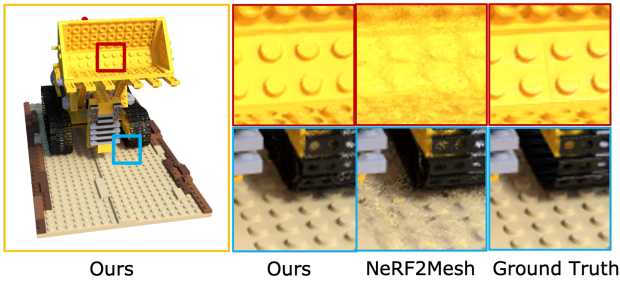


Figure 4: Visualization of rendering quality. Our method can render finer details compared to the NeRF2Mesh’s approach.

	PSNR $\uparrow$	SSIM $\uparrow$	LPIPS $\downarrow$
NVdiffrec	28.76	0.93	<b>0.049</b>
NeRF2Mesh	29.11	0.93	0.080
Ours (w/o refinement)	29.20	0.94	0.074
Ours	<b>29.42</b>	<b>0.94</b>	0.072

Table 2: Rendering quality comparisons on the NeRF-synthetic dataset. Compared to NVdiffrec and NeRF2Mesh, our method achieves better rendering quality.

The reward for an action at time  $t$  is defined as follows. During the  $t$ -th iteration, we select the optimal action (viewpoint combination) and add it to the original training set. The model is then trained for one iteration using both the enhanced training set (with the added viewpoints) and the original training set separately.

After training of this iteration, the mesh rendering quality is evaluated on the validation set by calculating the Peak Signal-to-Noise Ratio (PSNR) for both models. The reward for the action is determined by the difference in PSNR between the two models trained with enhanced training set and the original training set, with this difference serving as the reward for that action during the  $t$ -th iteration. The reward  $r_a(t)$  is formally defined as:

$$r_a(t) = \text{PSNR}_{\text{enhanced},a}(t) - \text{PSNR}_{\text{original}}(t) \quad (7)$$

### 3.4 Geometry and Appearance Refinement (Stage 2)

In the second stage, we perform refinement of the SDF grid and the appearance representation based on the surface rendering of the mesh. For each training iteration, we take two steps. We first select the optimal combination of viewpoints to enhance the training dataset based on our UCB strategy. We then adopt FlexiCubes to differentially extract the mesh from the SDF and nvdiffrast (Munkberg et al. 2022) to perform differentiable rendering, ensuring the continuity of gradient flow.

The core of FlexiCubes involves adding two attributes to each vertex in an SDF grid, namely weight and deformation, ensuring the SDF grid is deformable. These attributes

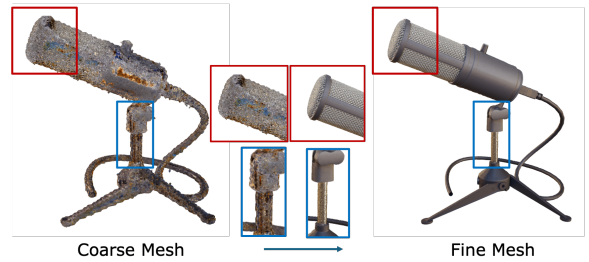


Figure 5: Fine mesh compared to the coarse mesh.

allow for the extraction of a mesh’s geometry based on positions of grid vertices and their respective SDF values. After extracting the mesh from the SDF grid, its appearance is determined by querying the appearance field. The mesh is then rendered using nvdiffrast, a differentiable rasterizer. The resulting rendering loss serves to optimize the attributes of FlexiCubes and the SDF values, while simultaneously updating the appearance field, allowing for flexible adjustments to the mesh vertices and their connectivity.

**Loss Function** In stage 2, we utilize the Charbonnier loss (Barron et al. 2022), replacing the loss function used in stage 1. The Charbonnier loss is defined as:

$$L_{\text{Charbonnier}}(x) = \sqrt{(x - x^*)^2 + \epsilon^2} \quad (8)$$

where  $x$  is the predicted value,  $x^*$  is the ground truth value, and  $\epsilon$  is a small constant that smooths the loss near zero, offering better handling of outliers. This loss function helps to achieve more stable and accurate convergence during training.

**Regularization** We apply Total Variation (TV) regularization (Chen et al. 2022) on the SDF grid to reduce floaters and enhance the smoothness of the SDF grid. We also employ the regularizer  $L_{\text{dev}}$  of FlexiCubes to reduce artifacts from the optimized mesh.

## 4 Experiments

### 4.1 Implementation Details

In the first stage, we set the training parameters identical to those used in NeRF2Mesh, training the NeRF model for 30,000 steps. At the end of the training, we extract an SDF grid at a resolution of  $128^3$ . For stage 2, we train the model for 600,000 steps to ensure that both the UCB and the model converge. The optimizer used is Adam, with the learning rates for both the FlexiCubes parameters and the SDF set to  $1 \times 10^{-4}$ . The experiments are all conducted on a high-performance computing platform equipped with a GeForce RTX 3090 GPU. For additional details, please refer to the supplementary materials section.

**Datasets** To evaluate the effectiveness of our approach, we utilize the NeRF-synthetic (Mildenhall et al. 2020) dataset to assess both the reconstructed mesh quality and the rendering quality. Experimental results demonstrate that our approach achieves excellent rendering and mesh reconstruction outcomes across all eight synthetic scenes.

VE	RF	PSNR $\uparrow$	SSIM $\uparrow$	LPIPS $\downarrow$
✓	✓	<b>29.42</b>	<b>0.94</b>	<b>0.072</b>
✗	✓	29.20	0.94	0.074
✗	✗	15.43	0.72	0.27

Table 3: Ablation study of our design choices. The results show that both the mesh refinement (RF) and viewpoint enhancement (VE) improve the overall performances.

	PSNR $\uparrow$	SSIM $\uparrow$	LPIPS $\downarrow$
Ours (UCB)	<b>29.42</b>	<b>0.94</b>	<b>0.072</b>
Greedy	29.18	0.92	0.078
Random	29.38	0.94	0.073

Table 4: Ablation study of our viewpoint enhancement strategies. Our UCB strategy outperforms both random and greedy strategies.

## 4.2 Evaluation

**Mesh Quality** To evaluate the geometric accuracy of our mesh reconstructions, we utilize the Chamfer Distance (CD) metric as done in NVdiffrec and NeRF2Mesh which quantifies the average closest point distance between the vertices of the reconstructed mesh and the ground truth. We establish NVdiffrec, MobileNeRF, Neus2 and NeRF2Mesh as baselines for our experiments and find that our results significantly outperform the previous works. The detailed outcomes of our mesh reconstruction are presented in Table 1 and Figure 3.

**Rendering Quality** We employ PSNR (Peak Signal-to-Noise Ratio), SSIM (Structural Similarity Index Measure), and LPIPS (Learned Perceptual Image Patch Similarity) metrics to evaluate the rendering quality of our mesh reconstruction. Compared to NVdiffrec and NeRF2Mesh, our methodology demonstrated superior performance in the majority of the tested scenes. The detailed results of this comparative analysis are presented in Table 2 and Figure 4. These metrics collectively assess the accuracy, visual similarity, and perceptual quality of the rendered images, highlighting our approach’s advancements in delivering high-fidelity reconstructions across various complex scenarios.

## 4.3 Ablation Studies

We conduct an ablation study to evaluate the effectiveness of our mesh refinement method and the online UCB adaptive viewpoint enhancement strategy. Specifically, we compare the performance of full model against variants excluding mesh refinement (RF) and viewpoint enhancement (VE), and further assess the UCB strategy’s effectiveness by comparing it to random and greedy viewpoint selection strategies. In the greedy viewpoint selection strategy, we select viewpoints closest to the highest loss viewpoint in each training iteration.

As shown in Table 3, when viewpoint enhancement is re-

moved, the rendering quality decreases, primarily because the model lacks the ability to incorporate diverse perspectives that contribute to more detailed and accurate reconstructions. When mesh refinement is further removed, there is a significant decline in the rendering quality of the mesh. The comparison between fine mesh and coarse mesh is shown in Figure 5.

The UCB strategy outperforms both random and greedy selection methods, as shown in Table 4. This is because the greedy approach tends to overfit to the currently known best viewpoints, potentially missing out on more informative perspectives. In contrast, the UCB method effectively balances exploration and exploitation, allowing for the online selection of the optimal combination of viewpoints.

## 5 Limitations and Conclusions

Although our proposed method shows improvements in rendering quality and mesh reconstruction compared to previous work, there are several limitations to acknowledge. We adopt the appearance field representation from NeRF2Mesh, which uses shallow MLPs and an appearance feature grid to model view-dependent effects. This approach may not effectively represent complex view-dependent components and fails to capture semi-transparent effects within scenes.

In summary, we introduce a novel mesh refinement algorithm and an online reinforcement learning strategy based on the UCB algorithm to adaptively enhance viewpoints, aim at improving mesh reconstruction from multi-view images. Our method initiates with training a NeRF to obtain a coarse SDF and an appearance field. Subsequently, by employing differentiable mesh extraction and rendering techniques, we optimize the model to produce the final polygonal mesh. Through our innovative algorithm and strategy, we achieve significant enhancements in both mesh rendering and mesh reconstruction outcomes. Additionally, our UCB algorithm is general and can be integrated into any NeRF-based mesh reconstruction framework.

## References

- Auer, P.; Cesa-Bianchi, N.; and Fischer, P. 2002. Finite-time analysis of the multiarmed bandit problem. *Machine learning*, 47: 235–256.
- Barron, J. T.; Mildenhall, B.; Verbin, D.; Srinivasan, P. P.; and Hedman, P. 2022. Mip-nerf 360: Unbounded anti-aliased neural radiance fields. In *Proceedings of the IEEE/CVF conference on computer vision and pattern recognition*, 5470–5479.
- Barron, J. T.; Mildenhall, B.; Verbin, D.; Srinivasan, P. P.; and Hedman, P. 2023. Zip-nerf: Anti-aliased grid-based neural radiance fields. In *Proceedings of the IEEE/CVF International Conference on Computer Vision*, 19697–19705.
- Chen, A.; Xu, Z.; Geiger, A.; Yu, J.; and Su, H. 2022. Tensorf: Tensorial radiance fields. In *European conference on computer vision*, 333–350. Springer.
- Chen, Z.; Funkhouser, T.; Hedman, P.; and Tagliasacchi, A. 2023. Mobilenerf: Exploiting the polygon rasterization

- pipeline for efficient neural field rendering on mobile architectures. In *Proceedings of the IEEE/CVF Conference on Computer Vision and Pattern Recognition*, 16569–16578.
- Fridovich-Keil, S.; Meanti, G.; Warburg, F. R.; Recht, B.; and Kanazawa, A. 2023. K-planes: Explicit radiance fields in space, time, and appearance. In *Proceedings of the IEEE/CVF Conference on Computer Vision and Pattern Recognition*, 12479–12488.
- Fridovich-Keil, S.; Yu, A.; Tancik, M.; Chen, Q.; Recht, B.; and Kanazawa, A. 2022. Plenoxels: Radiance fields without neural networks. In *Proceedings of the IEEE/CVF conference on computer vision and pattern recognition*, 5501–5510.
- Hasselgren, J.; Hofmann, N.; and Munkberg, J. 2022. Shape, light, and material decomposition from images using monte carlo rendering and denoising. *Advances in Neural Information Processing Systems*, 35: 22856–22869.
- Jin, L.; Chen, X.; Rückin, J.; and Popović, M. 2023. Neunbv: Next best view planning using uncertainty estimation in image-based neural rendering. In *2023 IEEE/RSJ International Conference on Intelligent Robots and Systems (IROS)*, 11305–11312. IEEE.
- Ju, T.; Losasso, F.; Schaefer, S.; and Warren, J. 2002. Dual contouring of hermite data. In *Proceedings of the 29th annual conference on Computer graphics and interactive techniques*, 339–346.
- Kim, H.; Yang, H.; Kim, T.; Kim, Y.; Kim, J.-H.; and Zhang, B.-T. 2024. ActiveNeuS: Active 3D Reconstruction using Neural Implicit Surface Uncertainty. *arXiv preprint arXiv:2405.02568*.
- Kong, F.; Wilson, N.; and Shadden, S. 2021. A deep-learning approach for direct whole-heart mesh reconstruction. *Medical image analysis*, 74: 102222.
- Krainin, M.; Curless, B.; and Fox, D. 2011. Autonomous generation of complete 3D object models using next best view manipulation planning. In *2011 IEEE international conference on robotics and automation*, 5031–5037. IEEE.
- Long, X.; Lin, C.; Wang, P.; Komura, T.; and Wang, W. 2022. Sparseneus: Fast generalizable neural surface reconstruction from sparse views. In *European Conference on Computer Vision*, 210–227. Springer.
- Lorensen, W. E.; and Cline, H. E. 1998. Marching cubes: A high resolution 3D surface construction algorithm. In *Seminal graphics: pioneering efforts that shaped the field*, 347–353.
- Lu, J.; Liu, F.; Girerd, C.; and Yip, M. C. 2023. Image-based pose estimation and shape reconstruction for robot manipulators and soft, continuum robots via differentiable rendering. In *2023 IEEE International Conference on Robotics and Automation (ICRA)*, 560–567. IEEE.
- McGreavy, C.; Kunze, L.; and Hawes, N. 2017. Next best view planning for object recognition in mobile robotics. In *CEUR Workshop Proceedings*, volume 1782. CEUR Workshop Proceedings.
- Mildenhall, B.; Srinivasan, P. P.; Tancik, M.; Barron, J. T.; Ramamoorthi, R.; and Ng, R. 2020. NeRF: Representing Scenes as Neural Radiance Fields for View Synthesis. *arXiv:2003.08934*.
- Mnih, V.; Kavukcuoglu, K.; Silver, D.; Rusu, A. A.; Veness, J.; Bellemare, M. G.; Graves, A.; Riedmiller, M.; Fidjeland, A. K.; Ostrovski, G.; et al. 2015. Human-level control through deep reinforcement learning. *nature*, 518(7540): 529–533.
- Müller, T.; Evans, A.; Schied, C.; and Keller, A. 2022. Instant neural graphics primitives with a multiresolution hash encoding. *ACM transactions on graphics (TOG)*, 41(4): 1–15.
- Munkberg, J.; Hasselgren, J.; Shen, T.; Gao, J.; Chen, W.; Evans, A.; Müller, T.; and Fidler, S. 2022. Extracting triangular 3d models, materials, and lighting from images. In *Proceedings of the IEEE/CVF Conference on Computer Vision and Pattern Recognition*, 8280–8290.
- Naazare, M.; Rosas, F. G.; and Schulz, D. 2022. Online next-best-view planner for 3D-exploration and inspection with a mobile manipulator robot. *IEEE Robotics and Automation Letters*, 7(2): 3779–3786.
- Navarro, F.; Fdez, J.; Garzón, M.; Roldán, J. J.; and Barrientos, A. 2018. Integrating 3D reconstruction and virtual reality: A new approach for immersive teleoperation. In *ROBOT 2017: Third Iberian Robotics Conference: Volume 2*, 606–616. Springer.
- Oechsle, M.; Peng, S.; and Geiger, A. 2021. Unisurf: Unifying neural implicit surfaces and radiance fields for multi-view reconstruction. In *Proceedings of the IEEE/CVF International Conference on Computer Vision*, 5589–5599.
- Pan, X.; Lai, Z.; Song, S.; and Huang, G. 2022. Activenerf: Learning where to see with uncertainty estimation. In *European Conference on Computer Vision*, 230–246. Springer.
- Rakotosaona, M.-J.; Manhardt, F.; Arroyo, D. M.; Niemeyer, M.; Kundu, A.; and Tombari, F. 2024. Nerfmeshing: Distilling neural radiance fields into geometrically-accurate 3d meshes. In *2024 International Conference on 3D Vision (3DV)*, 1156–1165. IEEE.
- Schulman, J.; Wolski, F.; Dhariwal, P.; Radford, A.; and Klimov, O. 2017. Proximal policy optimization algorithms. *arXiv preprint arXiv:1707.06347*.
- Shen, T.; Munkberg, J.; Hasselgren, J.; Yin, K.; Wang, Z.; Chen, W.; Gojcic, Z.; Fidler, S.; Sharp, N.; and Gao, J. 2023. Flexible Isosurface Extraction for Gradient-Based Mesh Optimization. *ACM Trans. Graph.*, 42(4): 37–1.
- Sun, C.; Sun, M.; and Chen, H.-T. 2022. Direct voxel grid optimization: Super-fast convergence for radiance fields reconstruction. In *Proceedings of the IEEE/CVF conference on computer vision and pattern recognition*, 5459–5469.
- Tang, J.; Zhou, H.; Chen, X.; Hu, T.; Ding, E.; Wang, J.; and Zeng, G. 2023. Delicate textured mesh recovery from nerf via adaptive surface refinement. In *Proceedings of the IEEE/CVF International Conference on Computer Vision*, 17739–17749.

Wang, N.; Zhang, Y.; Li, Z.; Fu, Y.; Liu, W.; and Jiang, Y.-G. 2018. Pixel2mesh: Generating 3d mesh models from single rgb images. In *Proceedings of the European conference on computer vision (ECCV)*, 52–67.

Wang, P.; Liu, L.; Liu, Y.; Theobalt, C.; Komura, T.; and Wang, W. 2021. Neus: Learning neural implicit surfaces by volume rendering for multi-view reconstruction. *arXiv preprint arXiv:2106.10689*.

Wang, Y.; Han, Q.; Habermann, M.; Daniilidis, K.; Theobalt, C.; and Liu, L. 2023. Neus2: Fast learning of neural implicit surfaces for multi-view reconstruction. In *Proceedings of the IEEE/CVF International Conference on Computer Vision*, 3295–3306.

Wu, J.; Liu, L.; Tan, Y.; Jia, Q.; Zhang, H.; and Zhang, X. 2023. ActRay: Online Active Ray Sampling for Radiance Fields. In *SIGGRAPH Asia 2023 Conference Papers*, 1–10.

Yariv, L.; Gu, J.; Kasten, Y.; and Lipman, Y. 2021. Volume rendering of neural implicit surfaces. *Advances in Neural Information Processing Systems*, 34: 4805–4815.